Chapter 1
Introduction

1.1 Motivation of the study

Over the past decades, the flow and heat transfer associated with a jet impinging onto a heated flat plate of various shapes have been the subject of many investigations because of its superior heat transfer capability. The results have been applied to improve the drying of textiles and paper, annealing of glass, cooling of gas turbine components and electronic equipments, freezing of tissue in cryosurgery, and many others. For some industrial applications, however, such as electronic cooling [1] and chemical vapor deposition [2], both high values and radial uniformity of heat and mass transfer rate are important. Besides, the flow needs to be stable and contain no vortices. The interest in the impinging gas jet confined in a chamber has accelerated recently because of the quick technological progresses in the growth of semiconductor thin crystal films on silicon wafers through rapid thermal processing (RTP) [3] and chemical vapor deposition (CVD) processes.

In order to obtain good thin film properties, the temperature uniformity of the wafer, appropriate geometry of vertical RTP and CVD chambers, suitable operating conditions and flow configuration are very important factors in designing the processors for the thin film growth [4]. Particularly, the flow recirculation in the processing chamber is detrimental to the film properties. Apparently, the structure of the vortex flow in the processing chamber is mainly affected by the jet inertia and the buoyancy force due to the heated wafer, along with the geometry of the chamber including the nozzle diameter, nozzle-to-wafer distance, wafer and chamber diameters. In the processing chambers three distinct flow regimes have been identified: (a) plug flow, where the gas flows smoothly over the substrate without any recirculation in the

chamber, (b) buoyancy-induced flow, where the buoyancy force associated with the heat substrate induces upward flow and recirculation of the gas, and (c) mixed flow, where the flow driven simultaneously by inertia and buoyancy forces. But, the details on how these parameters affect the vortex flow characteristics remain largely unexplored. In an initial attempt to examine the flow recirculation associated with the RTP processes Lin and his colleagues recently visualized the vortex flow of gas in a model vertical RTP processor [5] and found that the flow was dominated by the two axisymmetric vortex rolls. How the jet flow rate, jet-to-wafer temperature difference, and chamber pressure affected the vortex flow pattern was investigated in detail. In the present study a new experimental system with more precise flow and temperature control of the jet flow and heated wafer is established to explore the roles of the inertia and buoyancy forces in influencing various aspects of the vortex rolls. The detailed characteristics of the rolls driven simultaneously by the combined action of the inertia and buoyancy are to be delineated. In particular, the onset condition and the characteristics of the steady and time-dependent mixed convective vortex flow will be explored in detail. Besides, the detailed processes through which the vortex rolls are formed will be examined.

1.2 Literature review—heat transfer and flow characteristics of impinging Jets

Considerable amount of work from a number of research groups has been carried out in the past to study the fluid flow and heat transfer in the round or slot (two-dimensional) jet impinging onto a large horizontal plate. Most of the studies focus on quantifying the highly efficient heat transfer associated with the high speed impinging jets and the jets considered possess a much higher inertia force than the

buoyancy force generated by the temperature nonuniformify in the flow. Therefore the jet impinging flow is dominated by the jet inertia and some geometric parameters of the system. For instances, heat or mass transfer in the laminar and turbulent impinging jets was experimentally investigated by Gardon and Akfirat [6 & 7], Scholtz and Trass [8], Sparrow and Wang [9], Masliyah and Nguyen [10], and Hrycak [11]. Recently, the flow and thermal structures of the turbulent round jets were examined by Özdermir and Whitelaw [12] and Liu and Sullivan [13]. Moreover, the flow and heat transfer in the laminar impinging jets with the presence of an upper plate confinement were numerically predicted by Heiningen et al. [14], Saad et al. [15], and Law and Masliyah [16]. Besides, the results from the computation for the turbulent impinging jets were reported by Hosseinalipour and Mujumdar [17] and Morris and Garimella [18]. The corresponding heat transfer coefficient for the confined impinging jets was measured by Lin et al. [19]. A combined experimental and numerical study was recently conducted by Incropera and his colleagues [20 & 21] to explore the impinging liquid jets confined in a cylindrical container. The detailed flow characteristics in the impinging jets recently received considerable attention. The presence of a confinement plate above the target plate was noted to induce a big flow recirculation around the jet axis (Behnia et al. [22], Chua et al. [23], Voke and Gao [24]). The size and location of the recirculation center can be influenced by the jet Reynolds number and nozzle-to-plate spacing (Fitzgerald and Garimella [25], and Marple et al. [26]). The center of the flow recirculation was noted to move away from the jet axis when the nozzle-to-plate spacing was increased. This is in qualitative agreement with the experimental observation from Garimella and Rice [27]. The presence of the confinement plate is also known to restrict the jet flow entrainment from the surrounding, which reduces the jet spreading rate and leads to an increase in

the potential core length (Ashforth-Frost et al. [28], and Ashforth-Frost and Jambunathan [29]). Additionally, a low pressure region is induced near the impinging plate for single and double jets as the nozzle-to-plate spacing H/D is less than 2 (Baydar [30]). The pressure defect in the flow becomes more severe for a higher jet Reynolds number and a smaller nozzle-to-plate spacing. A round jet impinging onto a flat plate often results in double peaks in the Nusselt number distribution along the plate. The inner peak was considered to result from a local thinning of the boundary layer flow along the plate (Lee and Lee [31]) and it disappears for a large nozzle-to-plate spacing (Pamadi and Belov [32]). Lytle and Webb [33] and Li and Garimella [34] showed that the outer peak was more pronounced for a smaller nozzle-to-plate spacing and it moves radially outward for a higher jet Reynolds number. Schafer et al. [36] indicated that the outer heat transfer peak was due to the heat transfer enhancement associated with the secondary recirculation cell on the plate. Moreover, the flow in a confined jet was found to be dominated by a large recirculation vortex around the jet axis and a comparatively smaller adjacent secondary vortex right above the impinging plate (Law and Masliyah [16 & 35]). The location of the outer peak moves further away from the stagnation point at increasing jet Reynolds number but the location of the inner peak is independent of the Reynolds number (Colucci and Viskanta [37]).

The influences of the nozzle exit velocity profile on the impinging jet flow have been examined by Deshpande and Vaishnav [38]. Their results reveal that the peak values of the wall shear stress are lower for the uniform (flat) velocity profile. The results are attributed to the smaller momentum and kinetic energy for the same mass flux as compared with the parabolic velocity profile (fully developed velocity). Moreover, the potential core of the jet resulting from a fully developed velocity

profile is longer than that from a flat velocity profile (Ashforth-Frost et al. [28]). Recently, Huang and El-Genk [39] examined a swirling impinging jet and found that the swirl caused the flow to spread radially outward much more rapidly than without swirl. Besides, the swirl impinging jet induced markedly higher local and surface average Nusselt numbers and improved the radial uniformity of heat transfer on the impinged surface.

1.3 Literature Review—unsteady transitional impinging jets

More recently, the steady-to-unsteady flow transition for a confined laminar impinging jet (Re_j<1000) was numerically investigated by Chiriac and Ortega [40]. They pointed out that the critical jet Reynolds number for the onset of unsteady flow was between 585 and 610. The unsteady jet was characterized by a dominant frequency corresponding to the formation of shear layer vortices at the jet exit. More complete information on various characteristics of the impinging jets can be found from the recent critical reviews by Viskanta [41] and Jambunathan et al. [42]. It should be pointed out that in the above studies [6 - 40] the buoyancy force exhibits negligible effects on the jet flow. Recently, the importance of the buoyancy effects in a confined water impinging jet was illustrated by Ichimiya et al. [43] and a number of somewhat deformed buoyancy induced vortices were noted. Santen et al. [44, 45] indicated that the thermal instability for a confined jet impinging onto a heated circular plate did exist and the onset was affected by the Reynolds, Rayleigh and Prandtl numbers. Elison and Webb [46] found that during the transition between the laminar regime ($Re_j \le 1500$) and the turbulent regime ($Re_j \ge 1500$) the Nusselt number decreases for an increase in the jet Reynolds number. Some studies characterize the state of impinging jets according to jet's centerline turbulence

intensities. Lin et al. [19] measured the turbulence intensities in a confined slot jet and found that for $\mathrm{Re}_j < 1226$ the turbulent intensity is less than 5% at the stagnation point. The jet flow is considered to be laminar. As the jet Reynolds number gradually increases to 1226, the turbulence intensities at stagnation point increase sharply. Additionally, McNaughton and Sinclair [47] reported four characteristic jet regimes for circular free jets: dissipated-laminar jets for $\mathrm{Re}_j < 300$, fully laminar jets for $300 < \mathrm{Re}_j < 1000$, semi-turbulent jets for $1000 < \mathrm{Re}_j < 3000$, and fully turbulent jets for $\mathrm{Re}_j > 3000$.

1.4 Literature review—confined jet flow associated with CVD reactors and RTP processors

In the impinging jet flow encountered in the CVD and RTP processes, the gases input to the CVD reactors and RTP processors are at relatively low flowrates and the silicon wafer upon which semiconductor thin crystal films are grown and processed is at an elevated temperature. Under such circumstance the buoyancy in the flow is no longer small compared with the jet inertia. Significant flow recirculation can be induced by the buoyancy and the impinging jet flow is driven by the combined effects of inertia and buoyancy. The importance of the buoyancy on the recirculating flow in a vertical CVD reactor was demonstrated by Wahl [48]. Similar investigations have been carried out for various types of CVD reactors including the metal organic CVD [49-53] and single-wafer RTP processors [54, 55]. In these studies for the processing of the microelectronic circuits [45-55] various vortex flow patterns were reported in the jet impinging flow. Buoyancy induced symmetry breaking of the jet flow was also noted [53]. The optimal geometry of a MOCVD reactor was numerically investigated

by Kusumoto et al. [56]. They found that the optimal geometry for a larger flow rate should have a smaller inlet-to-pedestal spacing and a larger inlet pipe diameter. In addition, Santen et al. [57] reported nonuniform deposition rate caused by the nonuniformity of heat transfer resulting from a larger vortex roll near the cold side wall. Their data also shows that the rotating wafer and geometrical adjustments can be used to improve the deposition rate.

1.5 Objective of the present study

The above literature review clearly reveals that the detailed vortex flow and thermal characteristics associated with a mixed convective low speed vertical gas jet impinging onto a heated horizontal circular plate in a confined vertical chamber, which is directly related to the gas recirculation in CVD and RTP processes, are still poorly understood. In this study an experimental system is established to delineate how the inertia and buoyancy forces affect the vortex flow patterns in this confined impinging jet flow through the detailed flow visualization and transient temperature measurement. Attention is focused on the effects of the jet flow rate, the temperature difference between the heated plate and jet, and the geometry of the processing chamber, which includes diameter of the injection pipe and jet-to-disk separation distance, on the steady and time-dependent vortex flow patterns and their onset. Moreover, the formation of the inertia-driven rolls will be explored in detail.

Chapter 2

Experimental Apparatus and Procedures

In order to conduct the experiment at reasonably low cost, we use air as the working fluid to replace the inert gases normally employed in real CVD and RTP processes. In view of the similar thermodynamic and thermophysical properties for various gases, the results obtained here are still applicable to the CVD and RTP systems. The schematics of the experimental system established in the present study to investigate the mixed convective vortex flow characteristics resulting from a round air jet impinging vertically downwards onto a horizontal circular heated disk confined in a cylindrical chamber and the test section are respectively shown in Figs. 2.1 and 2.2. The system consists of four major parts – the processing chamber, temperature measurement and data acquisition unit, heating unit, and gas injection unit. The gas is first brought into the processing chamber through an injector and then injected directly onto a circular heated disk. The major parts are briefly described in the following.

2.1 Experimental apparatus

The processing chamber, which is made of 6-mm thick quartz glass to allow for the observation of the vortex flow pattern in it, is cylindrical and has a diameter of 291.0 mm and height of 200.0 mm between the chamber top and air exhaust located at the bottom of the chamber. Air is injected vertically downward from a long straight circular pipe into the cylindrical chamber along the axis of the chamber and impinges directly onto the heated disk. The air flows first over the heated disk, then moves through the annular section of the chamber, and finally leaves the chamber via twenty circular outlets of 12.7 mm in diameter opened at the bottom of the chamber. The

chamber is sealed to prevent any gas leakage. The top, bottom and side walls of the chamber are thermally well insulated to reduce the heat loss from the processing chamber to the ambient during the experiment. More specifically, the entire chamber is insulated with a superlon insulator of 100.0 mm thick. The insulator can be opened during the flow visualization experiment.

The heating unit is designed to maintain the circular disk at the preset uniform temperature during the experiment. A 25.0 mm thick high purity copper plate of eight-inch in diameter, acting as the disk, is directly placed on the heating elements. The heating unit consists of a resistance heating element, a holder and an insulator. The holder which is made of stainless steel can support the resistance heating element and copper disk at the high temperature. The heater attached onto the back side of the copper plate is divided into 3 concentric zones (Fig. 2.3). Each zone is independently heated by a power supply with the D.C. current passing through the nickel coil placed on the stainless steel holder. The entire heating unit is then placed on a Teflon plate. Additionally, to reduce the heat loss from the sidewall of the copper plate and Teflon plate, the lateral surface of the entire heating unit is wrapped with a 16.0 mm thick thermal insulation layer of superlon. A proper control of the voltage from each power supply allows us to maintain the copper plate at a nearly uniform temperature. Moreover, the copper plate temperature is measured by several corrected and calibrated T-type thermocouples at selected detection points located at 1-mm below the upper surface of the copper plate, which are fixed the detection points through the small holes drilled from the backside of the plate.

The gas injection unit consists of a 2HP air compressor, a flow meter, a smoke generator, filters, pressure regulator, connection pipes and injector. In the experiment, air is drawn from the ambient by the compressor and sent into a 300-liter and 100-psi

high-pressure air tank and is filtered to remove moisture and tiny particles. The installation of the high-pressure air tank is to suppress the fluctuation of the air flow and extends the life of the compressor. Then, the air is mixed with smoke tracers in the smoke generator, and regulated by the pressure regulator and is later injected into the processing chamber through the straight circular injection pipe which is coaxial with the processing chamber. The downward vertical air jet issuing from the pipe outlet impinges directly onto the heated plate. In the present study, two injection pipes with diameters, 10.0 and 22.1 mm, are tested and the straight portions of the pipes are both 600.0 mm long. The length of the injection pipes is selected to ensure that they are long enough to allow us to have a fully developed air flow at the exits of the injection pipes. The distance between the exits of the injection pipes and the heated disk is chosen to be 10.0 15.0, 20.0 and 30.0 mm. The air temperature at 600.0 mm upstream of the exits of the injection pipes is measured by a corrected and calibrated T-type thermocouple. The measured value is considered as the temperature of the air injected into the processing chamber since the whole injection pipe is thermally well insulated by a superlon insulation layer of 16.0-mm thick.

A smoke-tracer flow visualization technique is employed to observe the flow patterns resulting from the jet impinging onto the heated disk in the cylindrical chamber. The air flow pattern in the chamber is illuminated by the vertical and horizontal plane light sheets produced by passing parallel lights from an overhead projector through two adjustable knife edges. The experimental system is located in a darkroom to improve the contrast of the flow photos. The time variations of the flow pattern during the entire transient stage from the top and side views are recorded by the Sony digital video camera DCR-PC100. The recorded images are later examined carefully in a personal computer.

2.2 Analysis of time-average and instantaneous air temperature

To understand thermal characteristics of the steady and unsteady vortex flows, the temperature of the air flow in the processing chamber is measured by inserting a thermocouple probe into the chamber through twenty-four holes of 1-mm in diameter opened at the selected locations on the top of the chamber. In the experiment, the thermocouple tip is positioned at selected vertical distances from the upper surface of the disk. More specifically, the thermocouple probe is an OMEGA (model HYPO) mini hypodermic extremely small T-type thermocouple implanted in a 1 inch long stainless steel hypodermic needle.

2.3 Experimental procedures

For each case the experiment starts with the air at the room temperature T_a compressed first into the high pressure tank and the smoke generator through the connection pipe, and then injected into the processing chamber. The air moves over the disk and finally leaves the chamber through the twenty circular outlets at the bottom of the chamber. In the meantime the temperature of disk and the air flow rate are controlled at the preset levels. As the air flow in the processing chamber reaches steady or statistically stable state, we begin to visualize and record the vortex flow pattern in the chamber.

2.4 Uncertainty analysis

Uncertainties in the Rayleigh number, Reynolds number and other independent parameters are calculated according to the standard procedures established by Kline and McClintock [58]. The uncertainties of the thermophysical properties of the air are included in the uncertainty analysis. The properties of the working fluid (air) are

α=0.22(cm^2/s), β=0.0034 (1/k), ν=0.16 (cm^2/s) and Pr=0.72 at 30℃ and 1.0 bar. In addition, the uncertainties of the control unsteadiness and temperature nonuniformity of the heated disk are accounted for in the evaluation of the data uncertainty. The uncertainties of the temperature, volume flowrate, dimensions, Reynolds number and Rayleigh number measurements from this analysis are summarized in Table 2.1.

2.5 Verification of the experiment

To validate our experimental setup, the flow observed in the processing chamber for the limiting case when the disk is unheated (Ra=0) is compared with the numerical results from Law and Masliyah [16] for the impinging jet flow with the top plate confinement but without the sidewall confinement. The comparison is illustrated in Fig. 2.4 by showing the steady side view flow photo for an axisymmetric flow with the jet Reynolds number around 400 at D_j=10.0 mm and H/D_j=2. Note that in the region surrounding the jet axis the resulting vortex flow from our flow visualization is qualitatively the same as their numerical prediction. In the side wall region we have another circular vortex roll which results from the deflection of the boundary layer flow along the disk by the chamber side. But this is not seen in their prediction obviously due to the absence of a sidewall in their study. Thus, the experimental system established here is considered to be suitable for the present study.

Table 2.1 Summary of the uncertainty analysis

Parameter and Estimate Uncertainty	
Parameters	Uncertainty
D_j, D_w, H (m)	± 0.00005 m
T (℃)	± 0.2℃
ΔT (℃)	0.3℃
Q_j (slpm)	± 2%
μ (Nm/s^2) ρ (kg/m^3) υ (m^2/s)	± 0.05% ± 0.05% ± 0.07%
Ra	8.6%
Re_j	2.3%

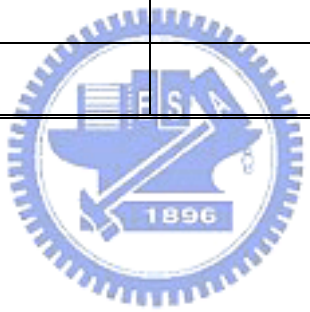

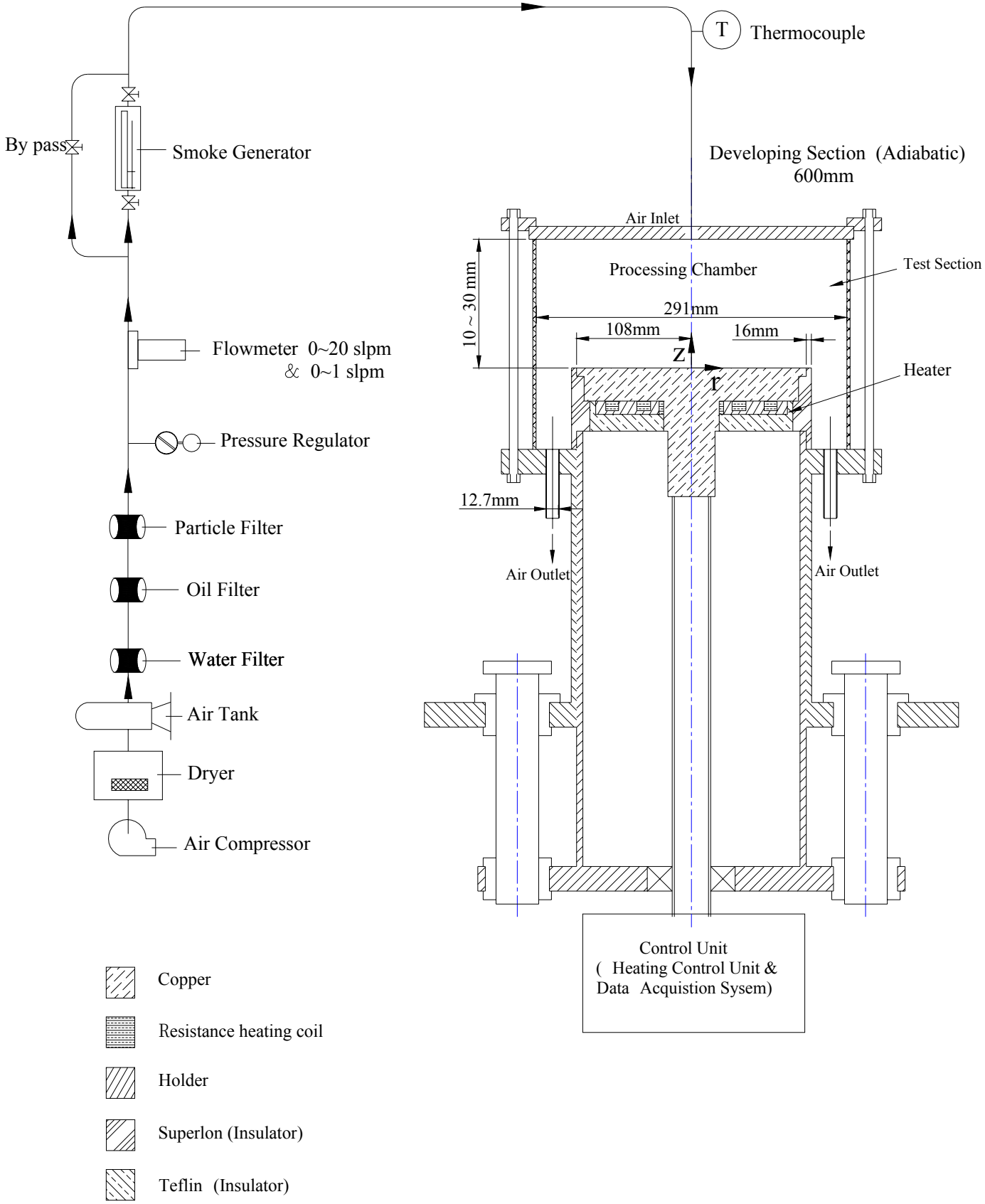

Fig. 2.1 Schematic diagram of the experimental system.

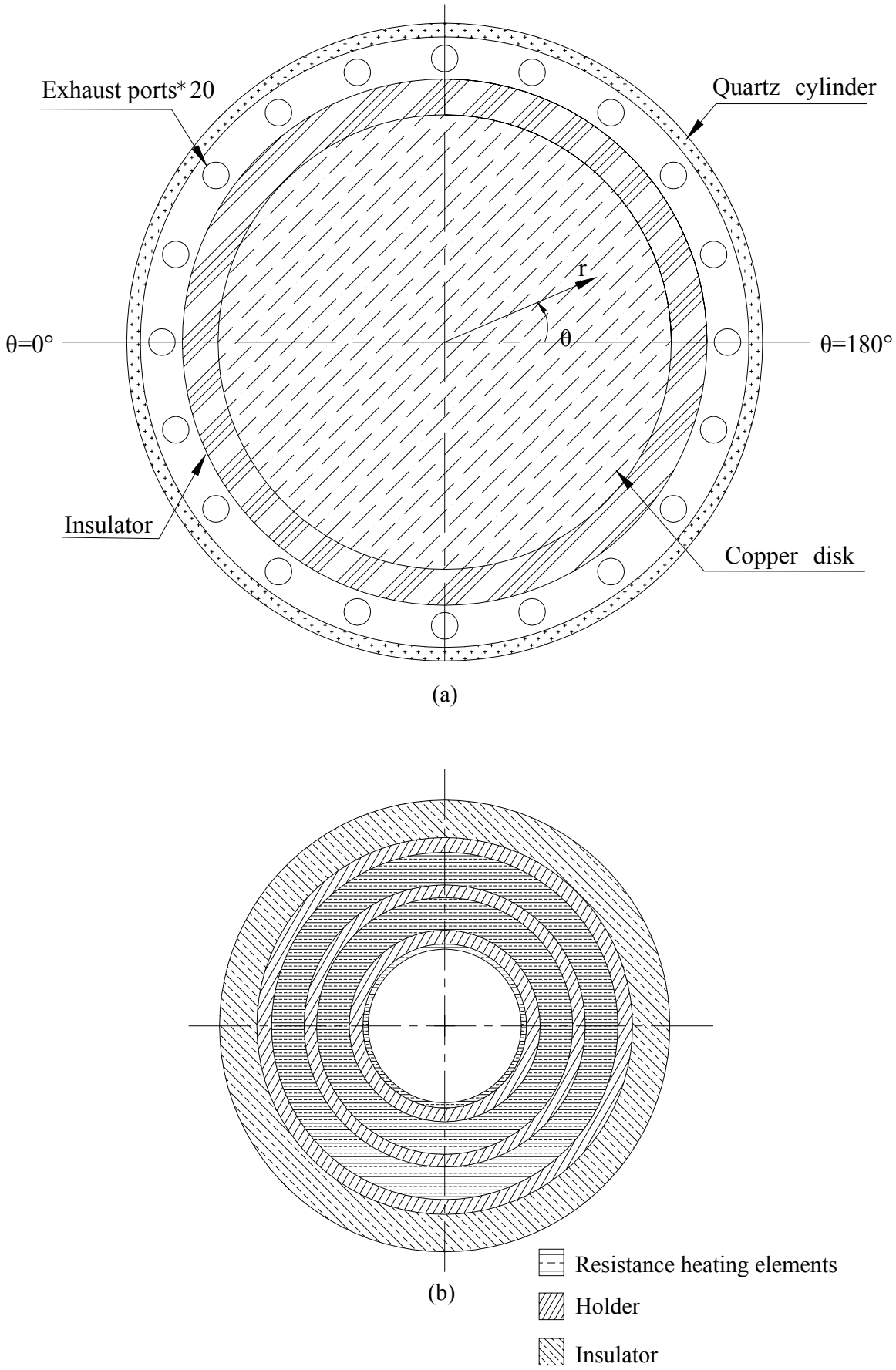

Fig. 2.2 Schematic of the test section from the top view (a) and 3-zone concentric heater (b).

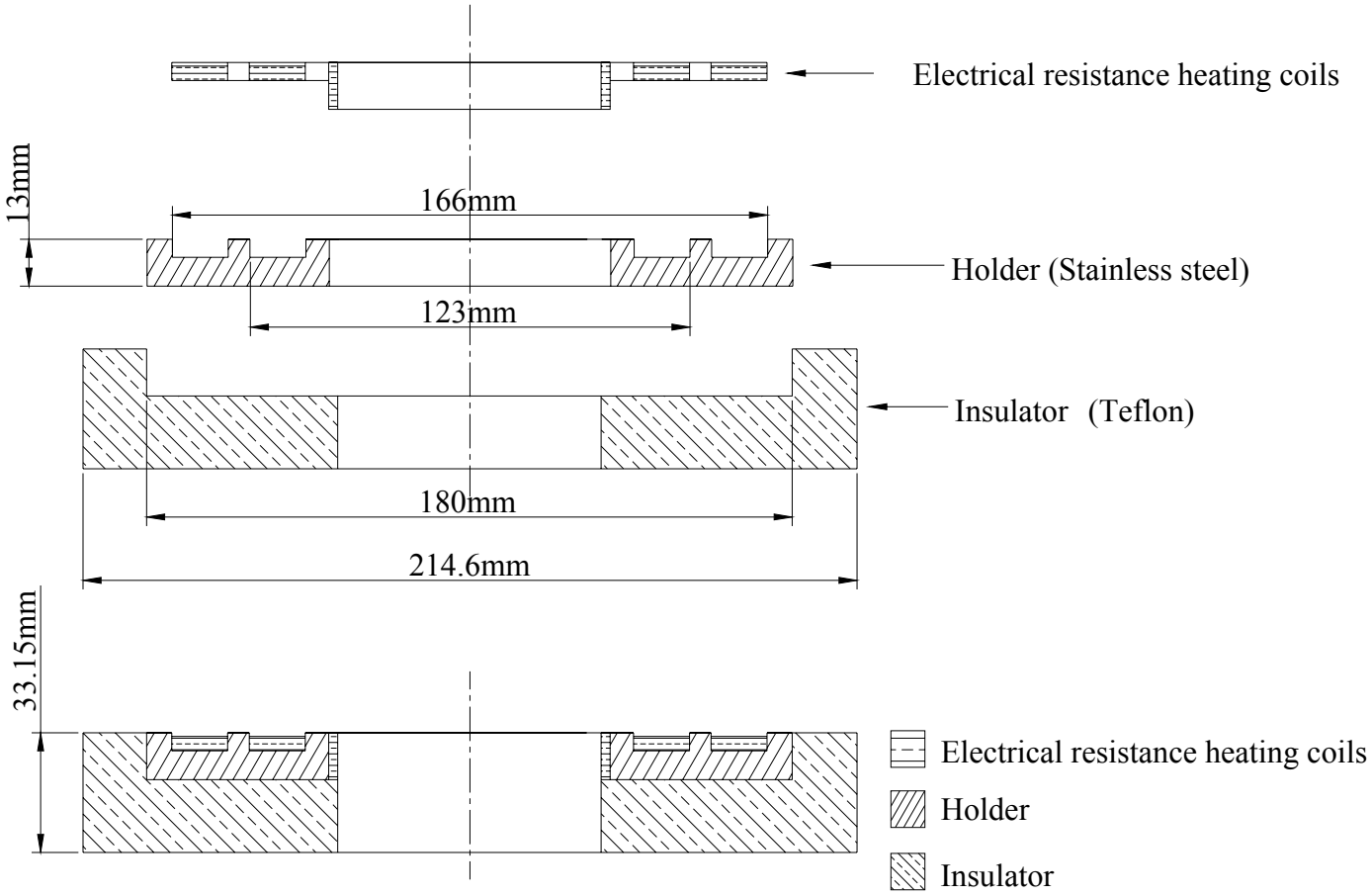

Fig. 2.3 The heater consists of three parts: resistance heating element, holder and insulator.

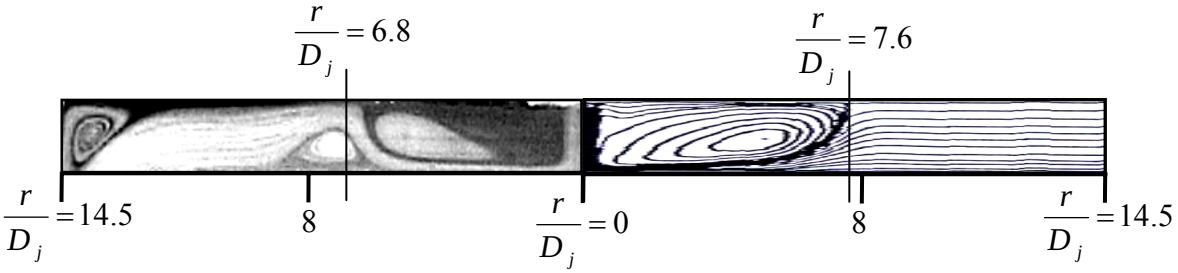

Fig. 2.4 The flow field for H/D_j=2 and Ra=0, left: the result from the present study at Re_j=406 for D_j=10.0 mm; right: contours of stream function from Law and Masliyah (1984) at Re_j=400.